Multi-Functional RIS: Signal Modeling and Optimization

Ailing Zheng, Wanli Ni, *Member, IEEE*, Wen Wang, Hui Tian, *Senior Member, IEEE*, Yonina C. Eldar, *Fellow, IEEE*, and Dusit Niyato, *Fellow, IEEE*

***Abstract*—In this paper, a multi-functional reconfigurable intelligent surface (MF-RIS) assisted non-orthogonal multiple access multiuser network is investigated. In contrast to existing studies assuming that the amplitude and phase shift coefficients of the refraction and reflection can be adjusted independently, we propose a practical model for the MF-RIS, where the refraction and reflection coefficients are highly coupled. Then, we investigate a sum-rate maximization problem by jointly optimizing the transmit beamforming and MF-RIS coefficients, subject to the coupled amplitude and phase shift constraints. To address the formulated non-convex problem, we propose an efficient iterative algorithm based on the fractional programming theory. Finally, numerical results show that: 1) The coupled MF-RIS scheme is superior to the simultaneous transmitting and reflecting RIS (STAR-RIS) and single-functional RIS (SF-RIS) schemes under the same power budget; 2) The performance gap between the ideal MF-RIS and coupled MF-RIS decreases with the increase of the total power budget.**

***Index Terms*—Multi-functional reconfigurable intelligent surface (MF-RIS), coupled amplitude and phase shift, non-orthogonal multiple access, rate maximization.**

I. Introduction

The dual-functional reconfigurable intelligent surface (DF-RIS), e.g., simultaneous transmitting and reflecting RIS (STAR-RIS) [1] or intelligent omni-surface (IOS) [2], has been proposed to overcome the topological constraints faced by the single-functional RIS (SF-RIS) [3]. The SF-RIS only reflects or refracts the incident signal to one side of the surface, which limits the flexibility and effectiveness of RIS [4]. By dividing the incident signal into reflection and refraction, the STAR-RIS is able to achieve a full-space reconfigurable wireless environment. However, the performance of STAR-RIS-aided networks is severely limited by the double-fading attenuation. Although active RISs with the signal amplification function have been proposed to tackle the double-fading issue [5], they restrict their service coverage to only one side of the surface. To address the above practical issues together, by introducing active load impedances, the multi-functional RIS (MF-RIS) was proposed to achieve signal amplification while maintaining a full-space signal manipulation [6]. Specifically, the incident signal is magnified by an amplifier embedded in each element of MF-RIS, thus effectively alleviating the double-fading attenuation and enhancing the signal strength [7], [8].

According to the equivalent surface current principle, to achieve signal refraction and reflection simultaneously, each element of MF-RIS should support electric and magnetic surface currents to enable flexible propagation environment control [9]. The two types of currents are determined by electric and magnetic impedences of MF-RIS elements. Existing studies on MF-RIS [6], [7], [8] assume that the amplitude and phase shift coefficients of refraction and reflection can be independently adjusted, where the arbitrary values of the corresponding electric and magnetic impedences need to be satisfied. This is non-trivial to realize in practice. The authors of [10] have studied the coupled phase shift model of STAR-RIS, where only the phase shifts of refraction and reflection are coupled while the amplitudes are changed randomly. However, with the amplification function, the amplitude and phase shift for MF-RIS are coupled [11], where the amplitude and the cosine of phase shift satisfy a specific constraint. Thus, the methods applied to STAR-RIS are unsuitable to handle the coupled amplitude and phase shift constraints faced by MF-RIS. For the real-world deployment of MF-RIS, it is necessary to design corresponding algorithms to address the above constraints, so that the optimized MF-RIS coefficients can be deployed directly on RIS hardware in the practical scenarios.

In this paper, we derive a coupled amplitude and phase shift model for the MF-RIS. Based on the proposed model, we investigate the design and optimization of an MF-RIS-aided network. The contributions are summarized as follows:

- We propose a coupled amplitude and phase shift model for MF-RIS. To study the impact of the proposed model on wireless networks, we investigate a resource allocation problem to maximize the sum-rate in an MF-RIS-aided non-orthogonal multiple access (NOMA) network.
- For the formulated non-convex problem, we propose an iterative algorithm to decompose it into transmit beamforming and MF-RIS coefficients subproblems by exploiting the fractional programming (FP) theory. Considering the coupled constraints, we separately optimize the amplitude and phase shift of MF-RIS coefficients. Then, Euler's formula is applied to transform the coupled constraints into a tractable form.
- Simulation results show that: 1) The coupled MF-RIS scheme outperforms the STAR-RIS and SF-RIS schemes under the same power budget with a substantial sum-rate gain of 42% and 94%, respectively; 2) Compared to STAR-RIS, the performance gap between the ideal MF-RIS scheme and the coupled MF-RIS scheme decreases as the total power budget increases.

II. Signal Model of MF-RIS

Let M as the number of MF-RIS elements. The refracted and reflected signal by the m-th element are given by $y_m^t = \beta_m^t e^{j\theta_m^t} s_m$ and $y_m^r = \beta_m^r e^{j\theta_m^r} s_m$, respectively, where s_m denotes the signal received on the m-th MF-RIS element, $m \in \mathcal{M} = \{1, 2, \ldots, M\}$. Here $\beta_m^{r/t} \in [0, \sqrt{\beta_{\max}}]$ and $\theta_m^{r/t} \in [0, 2\pi)$ represent the amplitude and phase shift of the m-th MF-RIS element, respectively, where $\beta_{\max} \geq 1$ denotes the maximum amplification factor and $(\beta_m^r)^2 + (\beta_m^t)^2 \leq \beta_{\max}$.

Based on the equivalent principle [9], each MF-RIS element has to support electric and magnetic current simultaneously to achieve the expected functions, which can be characterized by an equivalent electric and an equivalent magnetic circuit. Let $Z_{e,m}$ and $Z_{m,m}$ be the electric

Manuscript received 14 July 2023; revised 28 October 2023; accepted 4 November 2023. Date of publication 8 November 2023; date of current version 22 April 2024. This work was supported by the Natural Science Foundation of Shandong Province under Grant ZR2021LZH010. The review of this article was coordinated by Dr. Maged Elkashlan.*(Corresponding author: Hui Tian.)*

Ailing Zheng, Wen Wang, and Hui Tian are with the State Key Laboratory of Networking and Switching Technology, Beijing University of Posts and Telecommunications, Beijing 100876, China (e-mail: ailing.zheng@bupt.edu.cn; wen.wang@bupt.edu.cn; tianhui@bupt.edu.cn).

Wanli Ni is with the Department of Electronic Engineering, Tsinghua University, Beijing 100084, China (e-mail: charleswall@bupt.edu.cn).

Yonina C. Eldar is with the Faculty of Mathematics and Computer Science, Weizmann Institute of Science, Rehovot 7610001, Israel (e-mail: yonina.eldar@weizmann.ac.il).

Dusit Niyato is with the School of Computer Science and Engineering, Nanyang Technological University, Singapore 117583 (e-mail: DNIYATO@ntu.edu.sg).

Digital Object Identifier 10.1109/TVT.2023.3331093

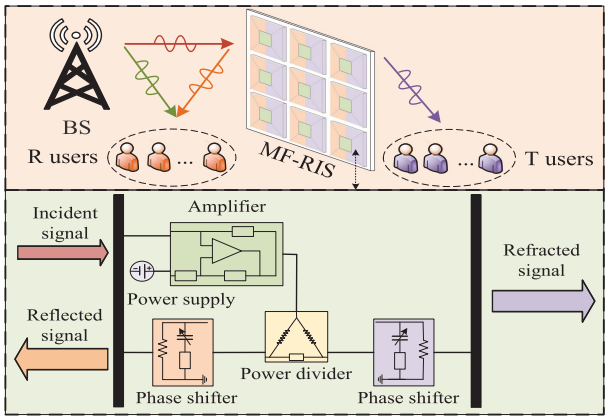

Fig. 1. Proposed MF-RIS assisted NOMA network.

and magnetic impedances of the m-th MF-RIS element. Then we obtain

$$T_m = \frac{2Z_{e,m}}{2Z_{e,m}+\eta} - \frac{Z_{m,m}}{Z_{m,m}+2\eta}, R_m = \frac{-\eta}{2Z_{e,m}+\eta} + \frac{Z_{m,m}}{Z_{m,m}+2\eta}, \tag{1}$$

where T_m and R_m represent the refraction and reflection coefficients of the m-th MF-RIS element, respectively. Here η is the free space wave impedance. The refraction and reflection coefficients are determined by the surface electric and magnetic impedances together. We reformulate (1) as

$$Z_{e,m} = \frac{\eta}{2}\frac{1+(R_m+T_m)}{1-(R_m+T_m)}, Z_{m,m} = 2\eta\frac{1+(R_m-T_m)}{1-(R_m-T_m)}, \tag{2}$$

which reveals the required surface electric and magnetic impedances to obtain refraction and reflection coefficients.

When the RIS is passive and lossless, the conservation of energy theory needs to be satisfied, which means that the energy of the incident signal is equal to the sum of the energies of the refracted and reflected signals, i.e., $(\beta_m^t)^2 + (\beta_m^r)^2 = 1$. In addition, the electric and magnetic impedances should be purely imaginary, i.e., $\Re(Z_{e,m}) = 0$ and $\Re(Z_{m,m}) = 0$ [10]. In this case, by introducing $T_m = \beta_m^t e^{\theta_m^t}$ and $R_m = \beta_m^r e^{\theta_m^r}$, the amplitude and phase shift coefficients satisfy $\beta_m^r \beta_m^t \cos(\theta_m^t - \theta_m^r) = 0$. However, when introducing negative resistances into RIS to achieve signal amplification, we may have $\Re(Z_{e,m}) \le 0$ and $\Re(Z_{m,m}) \le 0$ [12]. Thus, we obtain the coupled amplitude and phase shift model of the MF-RIS:

$$\frac{1-(\beta_m^r)^2-(\beta_m^t)^2}{2} \le \beta_m^r\beta_m^t\cos(\theta_m^t-\theta_m^r) \le \frac{(\beta_m^r)^2+(\beta_m^t)^2-1}{2}, \tag{3}$$

which indicates that the refraction and reflection coefficients are coupled. Moreover, we observe that the amplitudes of each element satisfy $(\beta_m^r)^2 + (\beta_m^t)^2 \ge 1$ with amplification ability. When the MF-RIS is in pure refraction or reflection mode, i.e., $\beta_m^r = 0$ or $\beta_m^t = 0$, the phase shifts can be chosen at random, where the amplitude coefficients satisfy $(\beta_m^r)^2 \ge 1$ or $(\beta_m^r)^2 \ge 1$.

III. System Model and Problem Formulation

We consider an MF-RIS assisted NOMA network, as shown in Fig. 1, where an N-antenna BS communicates with K single-antenna users with the help of an MF-RIS comprising M elements. The whole space is divided into refraction ($c = t$) and reflection ($c = r$) space, where $c \in \{t, r\}$. The set of users is denoted by $\mathcal{K} = \{1, 2, \ldots, K\}$, where the set of users in space c, i.e., $U_{c,k}$, is denoted by $\mathcal{K}_c = \{1, 2, \ldots, K_c\}$, satisfying $K = K_r + K_t$. Let $\mathbf{G} \in \mathbb{C}^{M\times N}$, $\mathbf{h}_{c,k} \in \mathbb{C}^{1\times M}$ and $\mathbf{f}_{c,k} \in \mathbb{C}^{1\times N}$ represent the channels from the BS to the MF-RIS, the MF-RIS to users, and the BS to users, respectively. To characterize the performance limit of the considered network, we assume that the channel state information of all channels is perfectly known at the BS by using existing channel estimation methods[1] [13]. Let $\mathbf{\Theta}_c = \text{diag}(\beta_1^c e^{j\theta_1^c}, \beta_2^c e^{j\theta_2^c}, \ldots, \beta_M^c e^{j\theta_M^c})$ as the refraction or reflection matrix of MF-RIS. The signal received at user $U_{c,k}$ is given by

$$y_{c,k} = (\mathbf{f}_{c,k} + \mathbf{h}_{c,k}\mathbf{\Theta}_c\mathbf{G})\sum_c\sum_{k=1}^{K_c}\mathbf{w}_{c,k}s_{c,k} + \mathbf{h}_{c,k}\mathbf{\Theta}_c\mathbf{z}_1 + z_2, \tag{4}$$

where $\mathbf{w}_{c,k}$ and $s_{c,k} \sim \mathcal{CN}(0,1)$ represent the transmit beamforming vector and the information symbol for user $U_{c,k}$, respectively. Here $\mathbf{z}_1 \sim \mathcal{CN}(0, \sigma_1^2\mathbf{I}_M)$ and $z_2 \sim \mathcal{CN}(0, \sigma_2^2)$ denote the thermal noise at the MF-RIS and users, respectively. According to NOMA protocol, the user with strong channel can mitigate the interference from the weak users by applying successive interference cancellation (SIC). Let $\mathbf{H}_{c,k} = \mathbf{f}_{c,k} + \mathbf{h}_{c,k}\mathbf{\Theta}_c\mathbf{G} \in \mathbb{C}^{1\times N}$. We assume that users' indexes in space c are ranked in an descending order, i.e.,

$$|\mathbf{H}_{c,1}\mathbf{w}_{c,1}|^2 \ge |\mathbf{H}_{c,2}\mathbf{w}_{c,2}|^2 \ge \ldots \ge |\mathbf{H}_{c,K_c}\mathbf{w}_{c,K_c}|^2. \tag{5}$$

Due to hardware limitation, the user may not always decode the signal perfectly. Thus, an error from the decoded signal may exist in the current user's signal. Then, the signal-to-interference-plus-noise-ratio (SINR) of user $U_{c,k}$ is given by

$$\gamma_{c,k} = \frac{|\mathbf{H}_{c,k}\mathbf{w}_{c,k}|^2}{\lambda\sum_{i=1}^{k-1}(|\mathbf{H}_{c,k}\mathbf{w}_{c,i}|^2) + I_{c,k} + I_{\bar{c},k} + \|\mathbf{h}_{c,k}\mathbf{\Theta}_c\mathbf{z}_1\|^2 + \sigma_2^2}, \tag{6}$$

where $I_{c,k}$ is the intra-space interference with $I_{c,k} = \sum_{i=k+1}^{K_c}|\mathbf{H}_{c,k}\mathbf{w}_{c,i}|^2$, and $I_{\bar{c},k}$ is the inter-space interference with $I_{\bar{c},k} = \sum_{i=1}^{K_{\bar{c}}}|\mathbf{H}_{c,k}\mathbf{w}_{\bar{c},i}|^2$ (if $c = r$, $\bar{c} = t$; otherwise $c = t$, $\bar{c} = r$). λ denotes the parameter of SIC decoding order error, where $\lambda = 0$ indicates perfect SIC. The data rate of user $U_{c,k}$ is given by $R_{c,k} = \log_2(1 + \gamma_{c,k})$.

In this paper, we aim to maximize the sum-rate of the MF-RIS assisted NOMA network by optimizing the transmit beamforming and MF-RIS coefficients simultaneously. The optimization problem is formulated as

$$\max_{\mathbf{w}_{c,k},\mathbf{\Theta}_c} \sum_c\sum_{k=1}^{K_c} R_{c,k} \tag{7a}$$

$$\text{s.t.} \sum_c\left(\sum_{\tilde{c}}\sum_{k=1}^{K_c}\|\mathbf{\Theta}_c\mathbf{G}\mathbf{w}_{\tilde{c},k}\|^2 + \|\mathbf{\Theta}_c\|_F^2\sigma_1^2\right) \le P_{\text{RIS}}, \tag{7b}$$

$$\sum_c(\beta_m^c)^2 \le \beta_{\max}, (\beta_m^c)^2 \in [0, \beta_{\max}], \theta_m^c \in [0, 2\pi), \tag{7c}$$

$$\sum_c\sum_{k=1}^{K_c}\|\mathbf{w}_{c,k}\|^2 \le P_{\text{BS}}, (3), (5), \tag{7d}$$

where $\tilde{c} \in \{r, t\}$, P_{BS} and P_{RIS} are the transmit power and amplification power at the BS and MF-RIS, respectively. Constraint (7b) and the first term in constraint (7d) represent the power budget constraints at the MF-RIS and BS, respectively. Due to the non-convex objective function (7a)

[1]We assume the MF-RIS does not perform signal amplification at the channel estimation stage. Thus, the MF-RIS reduces to the STAR-RIS, and the existing channel estimation method for STAR-RIS can be adopted [13].

and the highly coupled optimization variables, the formulated problem is challenging to solve directly. Inspired by FP theory, we propose a joint optimization framework to solve problem (7) efficiently in the following Section IV.

IV. Algorithm Design

We first transform the original problem into a tractable equivalent form by using FP theory. Then, the transmit beamforming and MF-RIS coefficients are designed alternately.

To deal with the sum-of-logarithms in problem (7), we decouple the optimization variables by exploiting FP methods [14]. By introducing auxiliary variables $\boldsymbol{\rho}_c = [\rho_{c,1}, \ldots, \rho_{K_c}]$ and $\boldsymbol{\tau}_c = [\tau_{c,1}, \ldots, \tau_{K_c}]$, problem (7) is given by

$$\max_{\mathbf{w}_{c,k}, \boldsymbol{\Theta}_c, \boldsymbol{\rho}_c, \boldsymbol{\tau}_c} R_{\text{sum}}(\mathbf{w}_{c,k}, \boldsymbol{\rho}_c, \boldsymbol{\tau}_c, \boldsymbol{\Theta}_c) = \sum_c \sum_{k=1}^{K_c} \ln(1+\rho_{c,k}) + \sum_c \sum_{k=1}^{K_c} \left(g(\mathbf{w}_{c,k}, \boldsymbol{\Theta}_c, \boldsymbol{\rho}_c, \boldsymbol{\tau}_c) - \rho_{c,k}\right) \tag{8a}$$

$$\text{s.t.} (7b\text{-}7d), \tag{8b}$$

where the function $g(\mathbf{w}_{c,k}, \boldsymbol{\Theta}_c, \boldsymbol{\rho}_c, \boldsymbol{\tau}_c)$ is defined as:

$$g(\mathbf{w}_{c,k}, \boldsymbol{\Theta}_c, \boldsymbol{\rho}_c, \boldsymbol{\tau}_c) = 2\sqrt{(1+\rho_{c,k})}\Re\{\tau_{c,k}^* \mathbf{H}_{c,k}\mathbf{w}_{c,k}\} - |\tau_{c,k}|^2 \left(\lambda \sum_{i=1}^{k-1}(|\mathbf{H}_{c,k}\mathbf{w}_{c,i}|^2) + \bar{I}_{c,k} + I_{\bar{c},k} + \|\mathbf{h}_{c,k}\boldsymbol{\Theta}_c\mathbf{z}_1\|^2 + \sigma_2^2\right), \tag{9}$$

and $\bar{I}_{c,k} = \sum_{i=k}^{K_c} |\mathbf{H}_{c,k}\mathbf{w}_{c,i}|^2$. According to the above transformation, we optimize $\{\boldsymbol{\rho}_c, \boldsymbol{\tau}_c\}$, $\{\mathbf{w}_{c,k}\}$, and $\{\boldsymbol{\Theta}_c\}$ alternatively to solve problem (8) in the following.

A. Auxiliary Variable Optimization

1) Fix $\{\mathbf{w}_{c,k}, \boldsymbol{\Theta}_c, \boldsymbol{\tau}_c\}$, and solve for $\boldsymbol{\rho}_c$. The optimal $\boldsymbol{\rho}_c$ is obtained by setting $\frac{\partial R_{\text{sum}}}{\partial \rho_{c,k}} = 0$, resulting in

$$\rho_{c,k}^{\text{opt}} = \frac{\varsigma_{c,k}{}^2 + \varsigma_{c,k}\sqrt{\varsigma_{c,k}^2 + 4}}{2}, \ \forall c, \ \forall k, \tag{10}$$

where $\varsigma_{c,k} = \Re\{\tau_{c,k}^* \mathbf{H}_{c,k}\mathbf{w}_{c,k}\}$.

2) Fix $\{\mathbf{w}_{c,k}, \boldsymbol{\Theta}_c, \boldsymbol{\rho}_c\}$, and solve for $\boldsymbol{\tau}_c$. The optimal $\boldsymbol{\tau}_c$ is obtained by setting $\frac{\partial R_{\text{sum}}}{\partial \tau_{c,k}} = 0$, resulting in

$$\tau_{c,k}^{\text{opt}} = \frac{\sqrt{1+\rho_{c,k}}\mathbf{H}_{c,k}\mathbf{w}_{c,k}}{\lambda \sum_{i=1}^{k-1}(|\mathbf{H}_{c,k}\mathbf{w}_{c,i}|^2) + \bar{I}_{c,k} + I_{\bar{c},k} + \|\mathbf{h}_{c,k}\boldsymbol{\Theta}_c\mathbf{z}_1\|^2 + \sigma_2^2}. \tag{11}$$

The computational complexity of updating $\boldsymbol{\rho}_c$ and $\boldsymbol{\tau}_c$ is $\mathcal{O}(KN)$ and $\mathcal{O}(K^2N + KM)$ [14], respectively.

B. Transmit Beamforming Design

With fixed $\{\boldsymbol{\Theta}_c, \boldsymbol{\tau}_c, \boldsymbol{\rho}_c\}$, problem (7) is recast as

$$\max_{\mathbf{w}_{c,k}} \sum_c \sum_{k=1}^{K_c} g(\mathbf{w}_{c,k}, \boldsymbol{\Theta}_c, \boldsymbol{\rho}_c, \boldsymbol{\tau}_c) \tag{12a}$$

$$\text{s.t.} \sum_c \sum_{k=1}^{K_c} \|\mathbf{w}_{c,k}\|^2 \le P_{\text{BS}}, (5), (7b). \tag{12b}$$

To solve problem (12), we define

$$\mathbf{A}_{c,k} = |\tau_{c,k}|^2 \mathbf{H}_{c,k}^{\text{H}}\mathbf{H}_{c,k}, \ \mathbf{b}_{c,k} = 2\sqrt{1+\rho_{c,k}}\tau_{c,k}^*\mathbf{H}_{c,k},$$
$$\mathbf{b} = [\mathbf{b}_{r,1}, \ldots, \mathbf{b}_{r,K_r}, \mathbf{b}_{t,1}, \ldots, \mathbf{b}_{r,K_t}]^{\text{H}},$$
$$\mathbf{w} = [\mathbf{w}_{r,1}^{\text{T}}, \ldots, \mathbf{w}_{r,K_r}^{\text{T}}, \mathbf{w}_{t,1}^{\text{T}}, \ldots, \mathbf{w}_{t,K_t}^{\text{T}}]^{\text{T}}. \tag{13}$$

Then, to handle constraint (5), we transform it as

$$|\mathbf{H}_{c,k}\mathbf{w}_{c,k}|^2 \ge \varepsilon_{c,k} = 2\Re\{\mathbf{w}_{c,k}^{\text{H},(\iota_1)}\mathbf{H}_{c,k}^{\text{H}}\mathbf{H}_{c,k}\mathbf{w}_{c,k}\} - |\mathbf{H}_{c,k}\mathbf{w}_{c,k}^{(\iota_1)}|^2.$$

Thus, problem (12) can be reformulated as follows:

$$\max_{\mathbf{w}} \Re\{\mathbf{b}^{\text{H}}\mathbf{w}\} - \sum_c \sum_{k=1}^{K_c} \mathbf{w}^{\text{H}}\overline{\mathbf{A}}_{c,k}\mathbf{w} \tag{14a}$$

$$\text{s.t.} \sum_c \sum_{k=1}^{K_c} \|\mathbf{w}_{c,k}\|^2 \le P_{\text{BS}}, \tag{14b}$$

$$\sum_c \mathbf{w}^{\text{H}}\mathbf{B}_c\mathbf{w} \le P_{\text{RIS}}^{\max}, \tag{14c}$$

$$\mathbf{w}_{c,k+1}^{\text{H}}\mathbf{H}_{c,k+1}^{\text{H}}\mathbf{H}_{c,k+1}\mathbf{w}_{c,k+1} \le \varepsilon_{c,k}, \tag{14d}$$

where we have $\mathbf{B}_c$, $P_{\text{RIS}}^{\max}$ and $\overline{\mathbf{A}}_{c,k}$:

$$\mathbf{B}_c = \mathbf{I}_K \otimes (\mathbf{G}^{\text{H}}\boldsymbol{\Theta}_c^{\text{H}}\boldsymbol{\Theta}_c\mathbf{G}), \ P_{\text{RIS}}^{\max} = P_{\text{RIS}} - \sum_c (\|\boldsymbol{\Theta}_c\|_F^2\sigma_1^2).$$

$$\overline{\mathbf{A}}_{c,k} = \text{diag}(\lambda\mathbf{A}_{c,1}, \ldots, \lambda\mathbf{A}_{c,(k-1)}, \mathbf{A}_{c,k}, \ldots, \mathbf{A}_{\bar{c},1}, \ldots, \mathbf{A}_{\bar{c},K_{\bar{c}}}).$$

Note that problem (14) is a standard quadratic constraint quadratic programming (QCQP) problem, which can be efficiently and optimally solved by CVX. Moreover, the computational complexity of solving $\mathbf{w}$ is $\mathcal{O}((KN)^3(M+2)^{1.5})$.

C. MF-RIS Coefficient Design

With given $\{\mathbf{w}_{c,k}, \boldsymbol{\tau}_c, \boldsymbol{\rho}_c\}$, we aim to optimize $\boldsymbol{\Theta}_c$. Considering $\boldsymbol{\beta}_m^c$ and θ_m^c are coupled, we have $\boldsymbol{\Theta}_c = \text{diag}(\boldsymbol{\beta}_c)\text{diag}(\mathbf{q}_c)$, where $\boldsymbol{\beta}_c = [\beta_1^c, \ldots, \beta_M^c]$ and $\mathbf{q}_c = [e^{j\theta_1^c}, \ldots, e^{j\theta_M^c}]$. Denoting $\boldsymbol{\beta} = [\boldsymbol{\beta}_r, \boldsymbol{\beta}_t]^{\text{T}}$, $\mathbf{q} = [\mathbf{q}_r, \mathbf{q}_t]^{\text{T}}$, we optimize $\boldsymbol{\beta}$ and $\mathbf{q}$ separately in the following.

1) Fix $\{\mathbf{w}_{c,k}, \boldsymbol{\tau}_c, \boldsymbol{\rho}_c, \mathbf{q}\}$, and solve for $\boldsymbol{\beta}$. The subproblem of $\boldsymbol{\beta}$ is reformulated as

$$\max_{\boldsymbol{\beta}} \sum_c \sum_{k=1}^{K_c} g(\mathbf{w}_{c,k}, \boldsymbol{\Theta}_c, \boldsymbol{\tau}_c, \boldsymbol{\rho}_c) \tag{15a}$$

$$\text{s.t.} \sum_c (\beta_m^c)^2 \le \beta_{\max}, 0 \le (\beta_m^c)^2 \le \beta_{\max}, (3), (5), (7b). \tag{15b}$$

Considering $(\beta_m^r)^2 + (\beta_m^t)^2 \ge 1$, we transform constraint (3) into $\left|2\beta_m^r\beta_m^t\cos(\theta_m^t - \theta_m^r)\right| \le (\beta_m^r)^2 + (\beta_m^t)^2 - 1$. Denoting $a_m = |2\cos(\theta_m^t - \theta_m^r)|$, we have

$$a_m\beta_m^r\beta_m^t \le (\beta_m^r)^2 + (\beta_m^t)^2 - 1. \tag{16}$$

However, constraint (16) is still non-convex. The upper bound of the left hand side of constraint (16) is given by $\beta_m^r\beta_m^t \le \frac{\alpha}{2}(\beta_m^r)^2 + \frac{1}{2\alpha}(\beta_m^t)^2$, where $\alpha = \beta_m^t/\beta_m^r$. Then, we apply the first-order Taylor expansion to get a lower bound of the term in the right hand side:

$$(\beta_m^r)^2 + (\beta_m^t)^2 \ge (\beta_m^{r,(\iota_1)})^2 + (\beta_m^{t,(\iota_1)})^2 + 2\beta_m^{r,(\iota_1)}(\beta_m^r - \beta_m^{r,(\iota_1)}) + 2\beta_m^{t,(\iota_1)}(\beta_m^t - \beta_m^{t,(\iota_1)}) \triangleq \vartheta_m^{(\iota_1)}. \tag{17}$$

Thus, constraint (16) is transformed into

$$a_m\left(\frac{\alpha}{2}(\beta_m^r)^2 + \frac{1}{2\alpha}(\beta_m^t)^2\right) \le \vartheta_m^{(\iota_1)} - 1. \tag{18}$$

Then, problem (15) is reformulated as

$$\max_{\boldsymbol{\beta}} \Re\{\mathbf{C}^{\mathrm{H}}\boldsymbol{\beta}\} - \boldsymbol{\beta}^{\mathrm{H}}\mathbf{D}\boldsymbol{\beta} \tag{19a}$$

$$\text{s.t.} \boldsymbol{\beta}^{\mathrm{H}}\mathbf{E}\boldsymbol{\beta} \le P_{\mathrm{RIS}}, \Upsilon_{c,k+1} \le \overline{\Upsilon}_{c,k}, \tag{19b}$$

$$\sum\nolimits_c (\beta_m^c)^2 \le \beta_{\max}, 0 \le (\beta_m^c)^2 \le \beta_{\max}, (18), \tag{19c}$$

where $\mathbf{C}, \mathbf{D}, \mathbf{E}, \overline{\Upsilon}_{c,k}$ and $\Upsilon_{c,k+1}$ are given in Appendix A. Thus, problem (19) can be easily solved via CVX.

2) Fix $\{\mathbf{w}, \boldsymbol{\tau}_c, \boldsymbol{\rho}_c, \boldsymbol{\beta}\}$, and solve for $\mathbf{q}$. The subproblem of $\mathbf{q}$ is reformulated as

$$\max_{\mathbf{q}} \sum\nolimits_c \sum\nolimits_{k=1}^{K_c} g(\mathbf{w}_{c,k}, \boldsymbol{\Theta}_c, \boldsymbol{\rho}_c, \boldsymbol{\tau}_c) \tag{20a}$$

$$\text{s.t.} |q_{c,m}| = 1, (3), (5), (7b). \tag{20b}$$

We define $\cos(\theta_m^t - \theta_m^r) = \cos\theta_m^t \cos\theta_m^r + \sin\theta_m^t \sin\theta_m^r = \Re(q_{t,m})\Re(q_{r,m}) + \Im(q_{t,m})\Im(q_{r,m}) \triangleq \Gamma$ by exploiting Euler's formula. Thus, constraint (3) is transformed as

$$\frac{1-(\beta_m^r)^2-(\beta_m^t)^2}{2\beta_m^r\beta_m^t} \le \Gamma \le \frac{(\beta_m^r)^2+(\beta_m^t)^2-1}{2\beta_m^r\beta_m^t}. \tag{21}$$

After some reformulation, problem (20) is transformed into

$$\max_{\mathbf{q}_c} \Re\{\overline{\mathbf{C}}^{\mathrm{H}}\mathbf{q}\} - \mathbf{q}^{\mathrm{H}}\overline{\mathbf{D}}\mathbf{q} \tag{22a}$$

$$\text{s.t.} \mathbf{q}^{\mathrm{H}}\overline{\mathbf{E}}\mathbf{q} \le P_{\mathrm{RIS}}, |q_{c,m}| = 1, \nu_{c,k+1} \le \bar{\nu}_{c,k}, (21), \tag{22b}$$

where $\overline{\mathbf{C}}, \overline{\mathbf{D}}, \overline{\mathbf{E}}, \bar{\nu}_{c,k}$ and $\nu_{c,k+1}$ are given in Appendix B.

Due to the non-convex constraints in (22b), problem (22) is still difficult to solve directly. By adopting penalty convex-concave procedure (CCP), the unit modules constraint in (22b) can be rewritten as $1 \le q_{c,m}^* q_{c,m} \le 1$. Then, we convert $1 \le q_{c,m}^* q_{c,m}$ into $1 \le 2\Re(q_{c,m}^* q_{c,m}^{(\iota_1)}) - q_{c,m}^{*,(\iota_1)} q_{c,m}^{(\iota_1)}$, where $q_{c,m}^{(\iota_1)}$ is the value of $q_{c,m}$ in the ι_1-th iteration. By introducing $2M$ slack variables $\mathbf{b} = [b_1, \ldots, b_{2M}]$, the unit modules constraint in (22b) is rewritten as

$$q_{c,m}^{*,(\iota_1)} q_{c,m}^{(\iota_1)} - 2\Re(q_{c,m}^* q_{c,m}^{(\iota_1)}) \le b_m - 1, q_{c,m}^* q_{c,m} \le 1 + b_{m+M}. \tag{23}$$

For constraint (21), the detailed derivation is given in Appendix C. Then, problem (22) is reformulated as

$$\max_{\mathbf{q},\mathbf{b}\ge\mathbf{0}} \Re\{\overline{\mathbf{C}}^{\mathrm{H}}\mathbf{q}\} - \mathbf{q}^{\mathrm{H}}\overline{\mathbf{D}}\mathbf{q} - \lambda^{(\iota_1)} \sum\nolimits_{m=1}^{2M} b_m \tag{24a}$$

$$\text{s.t.} \frac{(\beta_m^r)^2+(\beta_m^t)^2-1}{2\beta_m^r\beta_m^t} \ge \varrho_m, \mathbf{q}^{\mathrm{H}}\overline{\mathbf{E}}\mathbf{q} \le P_{\mathrm{RIS}}, \tag{24b}$$

$$\frac{1-(\beta_m^r)^2-(\beta_m^t)^2}{2\beta_m^r\beta_m^t} \le \omega_m, \nu_{c,k+1} \le \bar{\nu}_{c,k}, (5), \tag{24c}$$

where $\lambda^{(\iota_1)}$ is the regularization factor to control the feasibility of the constraints in the ι_1-th iteration. Here ϱ_m and ω_m are given in Appendix C. Problem (24) can be efficiently solved via CVX. Furthermore, the computational complexity of solving $\boldsymbol{\beta}$ and $\mathbf{q}$ is the same, e.g., $(M^3(M+1)^{1.5})$.

The solution of problem (7) can be obtained by solving (10), (11), (14), (19) and (24) alternately. Since the sum-rate monotonically increases over iterations and the transmit power is limited, the iterative algorithm is guaranteed to converge.

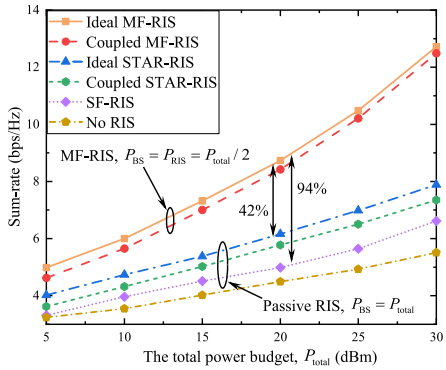

Fig. 2. Sum-rate versus P_{total} with $P_{\mathrm{RIS}} = P_{\mathrm{total}}/2$, $M = 100$ and $Y_{\mathrm{RIS}} = 50$.

V. Simulation Results

In the simulation, the BS and RIS are located at (0, 0, 0) and (5, 50, 20), respectively. We set $M = 100$, $N = 16$, $\beta_{\max} = 50$ dB, $\lambda = 0.1$, and $K_r = K_t = 3$. The users in the reflection and refraction space are randomly located on circles centered on (0,50,0) and (10,50,0) with a radius of 3 m, respectively. Besides, we assume all channels are Rician channel with a Rician factor 3 dB, where the path loss exponent of the BS-RIS, BS-users and RIS-users channels are 2.5, 3.5, 2.8, respectively. The path loss at the reference distance is -30 dB. Moreover, the noise power induced at RIS and users are set to $\sigma_1^2 = \sigma_2^2 = -80$ dBm. We set the total power budget $P_{\mathrm{total}} = 20$ dBm, where $P_{\mathrm{BS}} = P_{\mathrm{RIS}} = P_{\mathrm{total}}/2$ for the MF-RIS-aided networks, and $P_{\mathrm{BS}} = P_{\mathrm{total}}$ for the passive RIS-aided networks. For the performance comparison, we consider the following four benchmarks: 1) ideal MF-RIS; 2) ideal STAR-RIS [1]; 3) coupled STAR-RIS [10]; 4) SF-RIS, where one $M/2$ refracting-only and one $M/2$ reflecting-only RIS are deployed adjacent to each other.

Fig. 2 shows the sum-rate versus P_{total}. It can be observed that the MF-RIS always outperforms other schemes as P_{total} increases. Specifically, compared to STAR-RIS and SF-RIS, the MF-RIS obtains a performance gain of 42% and 94% when $P_{\mathrm{total}} = 20$ dBm, respectively. This can be explained as follows. When half the total power is allocated to RIS, this part of the power can amplify the incident signals attenuated after the transmission of the BS-RIS link. Thus, the outgoing signals only undergo the RIS-user link, which means that the power at RIS is only affected by the RIS-user link. Moreover, as P_{total} increases, the performance gap between the ideal MF-RIS and coupled MF-RIS decreases. Specifically, when P_{total} increases from 10 dBm to 30 dBm, the sum-rate of the ideal MF-RIS and coupled MF-RIS increase from 5.99 bps/Hz to 12.72 bps/Hz and from 5.65 bps/Hz to 12.48 bps/Hz, respectively. In other words, the performance gap decreases from 6% to 2%. This is because with the increase of the amplification gain, the coupling of amplitude and phase shift of each element becomes loose and approximately can be adjusted independently.

Fig. 3 plots the sum-rate versus M. When M increases from 10 to 100, the sum-rate of the ideal MF-RIS and STAR-RIS increases by 3.37 bps/Hz and 2.19 bps/Hz, respectively. This reveals that the performance gain obtained from MF-RIS is greater than the STAR-RIS by increasing M. Moreover, compared to SF-RIS, the MF-RIS and STAR-RIS can improve the sum-rate by 72% and 28%, respectively. We observe that the performance gap between the ideal MF-RIS and coupled MF-RIS is smaller than that between the ideal STAR-RIS and coupled STAR-RIS. It is reasonable that compared to STAR-RIS (i.e., $|\theta_m^r - \theta_m^t| = \frac{\pi}{2}$ or $\frac{3\pi}{2}$), the coupled amplitude and phase shift constraints of MF-RIS are easier to satisfy.

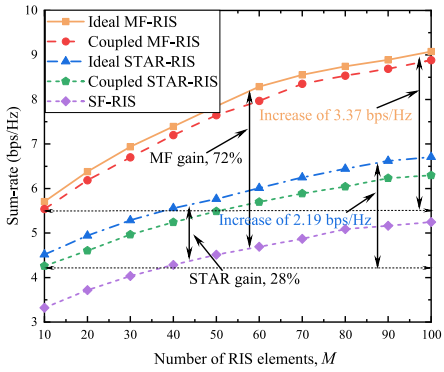

Fig. 3. Sum-rate versus M with $P_{\text{RIS}} = P_{\text{total}}/2 = 17$ dBm and $Y_{\text{RIS}} = 50$.

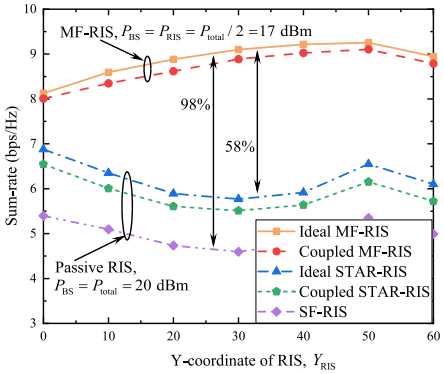

Fig. 4. Sum-rate versus Y_{RIS} with $P_{\text{RIS}} = P_{\text{total}}/2 = 17$ dBm and $M = 100$.

Fig. 4 investigates the sum-rate versus Y_{RIS}. The MF-RIS is able to alleviate the performance degradation caused by double-fading attenuation with the amplification function, which increases slowly with Y_{RIS} when $Y_{\text{RIS}} \leq 50$. However, when $Y_{\text{RIS}} \geq 50$, the sum-rate of MF-RIS decreases. The reason is that when MF-RIS moves away from both BS and users, the product of path loss for BS-RIS and RIS-users links increases rapidly, resulting in performance degradation. By contrast, due to the double-fading attenuation, the sum-rate of passive RISs first decrease and then increase. Moreover, the MF-RIS realizes a sum-rate gain of about 58% and 98% than the SATR-RIS and SF-RIS when $Y_{\text{RIS}} = 30$, respectively. Thus, compared to passive RISs, the MF-RIS can be deployed flexibly to ensure performance.

VI. Conclusion

In this work, a coupled amplitude and phase shift model for MF-RISs was provided. Then, we investigated a sum-rate maximization problem in an MF-RIS-aided NOMA network. An efficient iterative algorithm was proposed to solve the formulated non-convex problem by applying FP theory, where the transmit beamforming and MF-RIS coefficients were optimized alternately. Numerical results showed that MF-RIS schemes outperform STAR-RIS and SF-RIS schemes with 42% and 94% performance gains, respectively.

Appendix A
The Derivation for Solving Problem (15)

For problem (15), let $\mathbf{H}_{c,k}\mathbf{w}_{c,k} = (\mathbf{f}_{c,k} + \mathbf{h}_{c,k}\boldsymbol{\Theta}_c\mathbf{G})\mathbf{w}_{c,k} = (\mathbf{f}_{c,k} + \mathbf{h}_{c,k}\text{diag}(\boldsymbol{\beta}_c)\text{diag}(\mathbf{q}_c)\mathbf{G})\mathbf{w}_{c,k}$. We define

$$\bar{\mathbf{h}}_{c,k} = \mathbf{h}_{c,k}\text{diag}(\mathbf{q}_c),\ \overline{\mathbf{w}}_{c,k} = \text{diag}(\mathbf{G}\mathbf{w}_{c,k}),$$

and $\widetilde{\mathbf{h}}_{c,k} = \bar{\mathbf{h}}_{c,k}\overline{\mathbf{w}}_{c,k}$.

To tackle the non-convex objective function (15a), we denote $\mathbf{C}_c$ and $\mathbf{D}_c$ as follows:

$$\mathbf{C}_c = 2\sum_{k=1}^{K_c}\left(\sqrt{1+\rho_{c,k}}\Re(\tau_{c,k}^*\widetilde{\mathbf{h}}_{c,k}) - |\tau_{c,k}|^2 \left(\sum_{i=1}^{k-1}\lambda\Re(\bar{\mathbf{h}}_{c,k}\overline{\mathbf{w}}_{c,i}\mathbf{w}_{c,i}^{\text{H}}\mathbf{f}_{c,k}^{\text{H}}) + \boldsymbol{\Omega}_{c,k} + \boldsymbol{\Omega}_{\bar{c},k}\right)\right) \in \mathbb{C}^{1\times M}, \quad (25a)$$

$$\mathbf{D}_c = \sum_{k=1}^{K_c}|\tau_{c,k}|^2\left(\sum_{i=1}^{k-1}\lambda(\bar{\mathbf{h}}_{c,k}\overline{\mathbf{w}}_{c,i})^{\text{H}}(\bar{\mathbf{h}}_{c,k}\overline{\mathbf{w}}_{c,i}) + \overline{\boldsymbol{\Omega}}_{c,k} + \overline{\boldsymbol{\Omega}}_{\bar{c},k} + \left(\bar{\mathbf{h}}_{c,k}^{\text{H}}\bar{\mathbf{h}}_{c,k}\right)\sigma_1^2\right) \in \mathbb{C}^{M\times M}, \quad (25b)$$

where $\boldsymbol{\Omega}_{c,k} = \sum_{i=k}^{K_c}\Re(\bar{\mathbf{h}}_{c,k}\overline{\mathbf{w}}_{c,i}\mathbf{w}_{c,i}^{\text{H}}\mathbf{f}_{c,k}^{\text{H}})$, $\boldsymbol{\Omega}_{\bar{c},k} = \sum_{i=1}^{K_{\bar{c}}}\Re(\bar{\mathbf{h}}_{c,k}\overline{\mathbf{w}}_{\bar{c},i}\mathbf{w}_{\bar{c},i}^{\text{H}}\mathbf{f}_{c,k}^{\text{H}})$, $\overline{\boldsymbol{\Omega}}_{c,k} = \sum_{i=k}^{K_c}(\bar{\mathbf{h}}_{c,k}\overline{\mathbf{w}}_{c,i})^{\text{H}}(\bar{\mathbf{h}}_{c,k}\overline{\mathbf{w}}_{c,i})$, and $\overline{\boldsymbol{\Omega}}_{\bar{c},k} = \sum_{i=1}^{K_{\bar{c}}}(\bar{\mathbf{h}}_{c,k}\overline{\mathbf{w}}_{\bar{c},i})^{\text{H}}(\bar{\mathbf{h}}_{c,k}\overline{\mathbf{w}}_{\bar{c},i})$.

Then, we define $\mathbf{E}_c$, $\Upsilon_{c,k}$ and $\overline{\Upsilon}_{c,k}$ to handle constraints (5) and (7c) in the following:

$$\mathbf{E}_c = \sum_{\tilde{c}}\sum_{k=1}^{K_c}(\text{diag}(\mathbf{q}_c)\mathbf{G}\mathbf{w}_{\tilde{c},k})(\text{diag}(\mathbf{q}_c)\mathbf{G}\mathbf{w}_{\tilde{c},k})^{\text{H}} + \text{diag}(\mathbf{q}_c^{\text{H}})\text{diag}(\mathbf{q}_c)\sigma_1^2,\ |\mathbf{H}_{c,k}\mathbf{w}_{c,k}|^2 = |\mathbf{f}_{c,k}\mathbf{w}_{c,k}|^2 + 2\Re\{\widetilde{\mathbf{h}}_{c,k}(\mathbf{w}_{c,k}^{\text{H}}\mathbf{f}_{c,k}^{\text{H}})\boldsymbol{\beta}_c^{\text{H}}\} + |\widetilde{\mathbf{h}}_{c,k}\boldsymbol{\beta}_c^{\text{H}}|^2 \triangleq \Upsilon_{c,k}, \quad (26a)$$

$$|\widetilde{\mathbf{h}}_{c,k}\boldsymbol{\beta}_c^{\text{H}}|^2 \geq \upsilon_{c,k} = 2\Re\{\boldsymbol{\beta}_c^{(\iota_1)}\widetilde{\mathbf{h}}_{c,k}^{\text{H}}\widetilde{\mathbf{h}}_{c,k}\boldsymbol{\beta}_c^{\text{H}}\} - |\widetilde{\mathbf{h}}_{c,k}\boldsymbol{\beta}_c^{\text{H},(\iota_1)}|^2, \quad (26b)$$

$$\Upsilon_{c,k} \geq \overline{\Upsilon}_{c,k} = |\mathbf{f}_{c,k}\mathbf{w}_{c,k}|^2 + 2\Re\{\widetilde{\mathbf{h}}_{c,k}(\mathbf{w}_{c,k}^{\text{H}}\mathbf{f}_{c,k}^{\text{H}})\boldsymbol{\beta}_c^{\text{H}}\} + \upsilon_{c,k}. \quad (26c)$$

Finally, $\mathbf{C}$, $\mathbf{D}$ and $\mathbf{E}$ are given by

$$\mathbf{C} = [\mathbf{C}_r, \mathbf{C}_t]^{\text{H}},\ \mathbf{D} = \begin{bmatrix}\mathbf{D}_r & \\ & \mathbf{D}_t\end{bmatrix},\ \mathbf{E} = \begin{bmatrix}\mathbf{E}_r & \\ & \mathbf{E}_t\end{bmatrix}. \quad (27)$$

Appendix B
The Derivation for Solving Problem (20)

Similar to the transformation of $\boldsymbol{\beta}$, we define $\bar{\mathbf{f}}_{c,k} = \mathbf{h}_{c,k}\text{diag}(\boldsymbol{\beta}_c)$, and $\tilde{\mathbf{f}}_{c,k} = \bar{\mathbf{f}}_{c,k}\overline{\mathbf{w}}_{c,k} \in \mathbb{C}^{1\times M}$. Then, we denote $\overline{\mathbf{C}}_c$ and $\overline{\mathbf{D}}_c$ to tackle the non-convex objective function (20a):

$$\overline{\mathbf{C}}_c = 2\sum_{k=1}^{K_c}\left(\sqrt{1+\rho_{c,k}}\Re(\tau_{c,k}^*\tilde{\mathbf{f}}_{c,k}) - |\tau_{c,k}|^2\left(\sum_{i=1}^{k-1}\lambda\Re\left(\bar{\mathbf{f}}_{c,k}\overline{\mathbf{w}}_{c,i}\mathbf{w}_{c,i}^{\text{H}}\mathbf{f}_{c,k}^{\text{H}}\right) + \boldsymbol{\Xi}_{c,k} + \boldsymbol{\Xi}_{\bar{c},k}\right)\right), \quad (28a)$$

$$\overline{\mathbf{D}}_c = \sum_{k=1}^{K_c}|\tau_{c,k}|^2\left(\sum_{i=1}^{k-1}\lambda(\bar{\mathbf{f}}_{c,k}\overline{\mathbf{w}}_{c,i})^{\text{H}}\left(\bar{\mathbf{f}}_{c,k}\overline{\mathbf{w}}_{c,i}\right) + \widetilde{\boldsymbol{\Xi}}_{c,k} + \widetilde{\boldsymbol{\Xi}}_{\bar{c},k} + \left(\bar{\mathbf{f}}_{c,k}^{\text{H}}\bar{\mathbf{f}}_{c,k}\right)\sigma_1^2\right), \quad (28b)$$

where $\boldsymbol{\Xi}_{c,k} = \sum_{i=k}^{K_c}\Re(\bar{\mathbf{f}}_{c,k}\overline{\mathbf{w}}_{c,i}\mathbf{w}_{c,i}^{\text{H}}\mathbf{f}_{c,k}^{\text{H}})$, $\boldsymbol{\Xi}_{\bar{c},k} = \sum_{i=1}^{K_{\bar{c}}}\Re(\bar{\mathbf{f}}_{c,k}\overline{\mathbf{w}}_{\bar{c},i}\mathbf{w}_{\bar{c},i}^{\text{H}}\mathbf{f}_{c,k}^{\text{H}})$, $\widetilde{\boldsymbol{\Xi}}_{c,k} = \sum_{i=k}^{K_c}(\bar{\mathbf{f}}_{c,k}\overline{\mathbf{w}}_{c,i})^{\text{H}}(\bar{\mathbf{f}}_{c,k}\overline{\mathbf{w}}_{c,i})$, and $\widetilde{\boldsymbol{\Xi}}_{\bar{c},k} = \sum_{i=1}^{K_{\bar{c}}}(\bar{\mathbf{f}}_{c,k}\overline{\mathbf{w}}_{\bar{c},i})^{\text{H}}(\bar{\mathbf{f}}_{c,k}\overline{\mathbf{w}}_{\bar{c},i})$.

$$\omega_m \triangleq -\frac{1}{2}\left((\zeta_{r,m}^{R})^2+(\zeta_{t,m}^{R})^2\right)-\frac{1}{2}(\zeta_{r,m}^{R,(\iota_1)}+\zeta_{t,m}^{R,(\iota_1)})^2+\zeta_{r,m}^{R}(\zeta_{r,m}^{R,(\iota_1)}+\zeta_{t,m}^{R,(\iota_1)})+\zeta_{t,m}^{R}(\zeta_{r,m}^{R,(\iota_1)}+\zeta_{t,m}^{R,(\iota_1)})$$
$$-\frac{1}{2}\left((\zeta_{r,m}^{I})^2+(\zeta_{t,m}^{I})^2\right)-\frac{1}{2}(\zeta_{r,m}^{I,(\iota_1)}+\zeta_{t,m}^{I,(\iota_1)})^2+(\zeta_{r,m}^{I})(\zeta_{r,m}^{I,(\iota_1)}+\zeta_{t,m}^{I,(\iota_1)})+\zeta_{t,m}^{I}(\zeta_{r,m}^{I,(\iota_1)}+\zeta_{t,m}^{I,(\iota_1)}). \quad (31)$$

To handle constraints (5) and (7c) in problem (20), we define $\overline{\mathbf{E}}_c$, $\nu_{c,k}$ and $\overline{\nu}_{c,k}$ as follows:

$$\overline{\mathbf{E}}_c=\sum\nolimits_{\tilde{c}}\sum\nolimits_{k=1}^{K_c}(\mathrm{diag}(\boldsymbol{\beta}_c)\mathbf{G}\mathbf{w}_{c,k})(\mathrm{diag}(\boldsymbol{\beta}_c)\mathbf{G}\mathbf{w}_{c,k})^{\mathrm{H}}$$
$$+\mathrm{diag}(\boldsymbol{\beta}_c)\mathrm{diag}(\boldsymbol{\beta}_c^{\mathrm{H}})\sigma_1^2,\ |\mathbf{H}_{c,k}\mathbf{w}_{c,k}|^2=|\mathbf{f}_{c,k}\mathbf{w}_{c,k}|^2$$
$$+2\Re\{\tilde{\mathbf{f}}_{c,k}(\mathbf{w}_{c,k}^{\mathrm{H}}\mathbf{f}_{c,k}^{\mathrm{H}})\mathbf{q}_c^{\mathrm{H}}\}+|\widetilde{\mathbf{f}}_{c,k}\mathbf{q}_c^{\mathrm{H}}|^2\triangleq\nu_{c,k}, \quad (29a)$$
$$|\widetilde{\mathbf{f}}_{c,k}\mathbf{q}_c^{\mathrm{H}}|^2\geq\chi_{c,k}=2\Re\{\mathbf{q}_c^{(\iota_1)}\widetilde{\mathbf{f}}_{c,k}^{\mathrm{H}}\widetilde{\mathbf{f}}_{c,k}\mathbf{q}_c^{\mathrm{H}}\}-|\widetilde{\mathbf{f}}_{c,k}\mathbf{q}_c^{\mathrm{H},(\iota_1)}|^2, \quad (29b)$$
$$\nu_{c,k}\geq\bar{\nu}_{c,k}=|\mathbf{f}_{c,k}\mathbf{w}_{c,k}|^2+2\Re\{\tilde{\mathbf{f}}_{c,k}(\mathbf{w}_{c,k}^{\mathrm{H}}\mathbf{f}_{c,k}^{\mathrm{H}})\mathbf{q}_c^{\mathrm{H}}\}+\chi_{c,k}. \quad (29c)$$

Eventually, $\overline{\mathbf{C}}$, $\overline{\mathbf{D}}$ and $\overline{\mathbf{E}}$ are denoted as

$$\overline{\mathbf{C}}=[\overline{\mathbf{C}}_r,\overline{\mathbf{C}}_t]^{\mathrm{H}},\ \overline{\mathbf{D}}=\begin{bmatrix}\overline{\mathbf{D}}_r & \\ & \overline{\mathbf{D}}_t\end{bmatrix},\ \overline{\mathbf{E}}=\begin{bmatrix}\overline{\mathbf{E}}_r & \\ & \overline{\mathbf{E}}_t\end{bmatrix}. \quad (30)$$

APPENDIX C
THE DERIVATION FOR SOLVING CONSTRAINT (21)

To tackle constraint (21), considering $xy=\frac{1}{2}(x+y)^2-\frac{1}{2}(x^2+y^2)$, we have $xy\geq-\frac{1}{2}(x^2+y^2)+\frac{1}{2}(x^{(\iota_1)}+y^{(\iota_1)})^2+(x-x^{(\iota_1)})(x^{(\iota_1)}+y^{(\iota_1)})+(y-y^{(\iota_1)})(x^{(\iota_1)}+y^{(\iota_1)})$. Let $\zeta_{c,m}^{R}=\Re(q_{c,m})$ and $\zeta_{c,m}^{I}=\Im(q_{c,m})$. Then, a lower bound of the left hand side of constraint (21) is given in (31), which is at the top of this page. Furthermore, the upper bound of the right hand side of (21) is given by

$$\varrho_m\triangleq\frac{\varpi_1}{2}(\zeta_{r,m}^{R})^2+\frac{1}{2\varpi_1}(\zeta_{t,m}^{R})^2+\frac{\varpi_2}{2}(\zeta_{r,m}^{I})^2+\frac{1}{2\varpi_2}(\zeta_{t,m}^{I})^2, \quad (32)$$

where ϖ_1 and ϖ_2 are updated by $\varpi_1^{(\iota_1)}=\zeta_{t,m}^{R,(\iota_1-1)}/\zeta_{r,m}^{R,(\iota_1-1)}$, $\varpi_2^{(\iota_1)}=\zeta_{t,m}^{I,(\iota_1-1)}/\zeta_{r,m}^{I,(\iota_1-1)}$.

REFERENCES

[1] J. Xu, Y. Liu, X. Mu, and O. A. Dobre, "STAR-RISs: Simultaneous transmitting and reflecting reconfigurable intelligent surfaces," *IEEE Commun. Lett.*, vol. 25, no. 9, pp. 3134–3138, Sep. 2021.

[2] S. Zhang et al., "Intelligent omni-surfaces: Ubiquitous wireless transmission by reflective-refractive metasurfaces," *IEEE Trans. Wireless Commun.*, vol. 21, no. 1, pp. 219–233, Jan. 2022.

[3] W. Wang, W. Ni, H. Tian, Z. Yang, C. Huang, and K.-K. Wong, "Safeguarding NOMA networks via reconfigurable dual-functional surface under imperfect CSI," *IEEE J. Sel. Topics Signal Process.*, vol. 16, no. 5, pp. 950–966, Aug. 2022.

[4] W. Ni, X. Liu, Y. Liu, H. Tian, and Y. Chen, "Resource allocation for multi-cell IRS-aided NOMA networks," *IEEE Trans. Wireless Commun.*, vol. 20, no. 7, pp. 4253–4268, Jul. 2021.

[5] K. Zhi, C. Pan, H. Ren, K. K. Chai, and M. Elkashlan, "Active RIS versus passive RIS: Which is superior with the same power budget?," *IEEE Commun. Lett.*, vol. 26, no. 5, pp. 1150–1154, May 2022.

[6] A. Zheng, W. Ni, W. Wang, and H. Tian, "Enhancing NOMA networks via reconfigurable multi-functional surface," *IEEE Commun. Lett.*, vol. 27, no. 4, pp. 1195–1199, Apr. 2023.

[7] H. Luo, L. Lv, Q. Wu, Z. Ding, N. Al-Dhahir, and J. Chen, "Beamforming design for active IOS aided NOMA networks," *IEEE Wireless Commun. Lett.*, vol. 12, no. 2, pp. 282–286, Feb. 2023.

[8] Y. Ma, M. Li, Y. Liu, Q. Wu, and Q. Liu, "Optimization for reflection and transmission dual-functional active RIS-assisted systems," *IEEE Trans. Commun.*, vol. 71, no. 9, pp. 5534–5548, Sept. 2023.

[9] B. O. Zhu et al., "Dynamic control of electromagnetic wave propagation with the equivalent principle inspired tunable metasurface," *Sci. Rep.*, vol. 4, 2014, Art. no. 4971.

[10] J. Xu, Y. Liu, X. Mu, R. Schober, and H. V. Poor, "STAR-RISs: A correlated T&R phase-shift model and practical phase-shift configuration strategies," *IEEE J. Sel. Topics Signal Process.*, vol. 16, no. 5, pp. 1097–1111, Aug. 2022.

[11] S. Taravati, B. A. Khan, S. Gupta, K. Achouri, and C. Caloz, "Nonreciprocal nongyrotropic magnetless metasurface," *IEEE Trans. Antennas Propag.*, vol. 65, no. 7, pp. 3589–3597, Jul. 2017.

[12] B. O. Zhu and Y. Feng, "Passive metasurface for reflectionless and arbitary control of electromagnetic wave transmission," *IEEE Trans. Antennas Propag.*, vol. 63, no. 12, pp. 5500–5511, Dec. 2015.

[13] C. Wu, C. You, Y. Liu, X. Gu, and Y. Cai, "Channel estimation for STAR-RIS-aided wireless communication," *IEEE Commun. Lett.*, vol. 26, no. 3, pp. 652–656, Mar. 2022.

[14] Z. Zhang et al., "Active RIS vs. passive RIS: Which will prevail in 6G?," *IEEE Trans. Commun.*, vol. 71, no. 3, pp. 1707–1725, Mar. 2023.